



Role of Various Tool Pin Profiles in Friction Stir Welding of AA2024 Alloys

Bharat Singh, Kuldeep K. Saxena, Piyush Singhal, and Tilak C. Joshi

Submitted: 23 February 2021 / Revised: 18 May 2021 / Accepted: 11 June 2021 / Published online: 19 July 2021

In FSW, tool pin profile has a significant contribution on mechanical and microstructural properties of metallic joints. In the present work, various pin profiles such as conical, pedal, cylindrical with thread, triangular, square and pentagonal pins are used to join the AA2024 plates. Mechanical and microstructural characterization is done for welded plates using different pin profile tools. The mechanical properties such as percentage elongation, ultimate tensile strength (UTS), microhardness and impact strength are significantly improved, when plates are joined using square pin profile. The obtained joint efficiency is 78% using square pin profile tool. The percentage elongation, UTS and impact energy of joint made by square pin tool are measured as 15%, 362 MPa and 5.7 Joule, respectively, which are higher than the values obtained using other pin profiles. EBSD analysis was performed to know the microstructural changes, which are a cause of mechanical properties alteration. Analysis reveals that stirred zone exhibits the recrystallized fine grains with equiaxed structure, which is a result of dynamic recrystallization and heating during plastic deformation of the zone. Large fraction of HAGB is also observed in stirred zone, which is a cause of improved mechanical properties of the joint.

Keywords dynamic recrystallization, EBSD, friction stir welding, grain refinement, impact Energy, material testing, pin profile

1. Introduction

Aluminum is one of the most inexpensive and preferred metallic materials for a widespread range of engineering applications. It has combination of beneficial properties such as strong ductility and high strength-to-weight ratio. In order to enhance armed forces deployability and mobility, the production of lighter materials of troop carriers and fighting vehicles is increasing rapidly (Ref 1). In the manufacture of these vehicles, high-performance aluminum alloys are usually used to have absorption ability and structural strength against impacts and blast loadings. AA2024-T351 is an aerospace alloy hardened by precipitation with a nominal composition of 4.4Cu-0.6Mn-1.5Mg-balance aluminum (wt. percent) (Ref 2). It exhibits better fracture toughness, high structural strength and better ballistics properties (Ref 3). High thermal conductivity, coefficient of thermal expansion (approx. two times of steel) and reactivity make aluminum alloys difficult to weld. The heat input associated with fusion welding process leads to high residual stresses which results in distortion of the part (Ref 4, 5). These associated difficulties could be avoided or minimized up to significant extent by the use of friction stir welding (FSW) technique which was invented in 1991 (Ref 6). The joint made

by FSW process is 34% stronger than joint produced by fusion welding process (Ref 7). In FSW process, tool design or the geometry of tool plays a vital role in deciding the heat generation, material flow and quality of the weld joint (Ref 8-10). Many developments in the design of FSW tools are well reported in the literature (Ref 11-13). Design of FSW tool includes profile of tool pin, shoulder, static volume and material used to make it (Ref 14). The goals of developments in the design of tool are to reduce process forces and to have better properties of joint and ease in the weld control and robustness of the process (Ref 15, 16). Dong et al. studied (Ref 17) the effect of stationary shoulder during friction stir welding and observed defect-free joints with better surface roughness approx. 53% reduction in surface roughness. Khodaverdizadeh et al. (Ref 18) investigated the pin profile effects on microstructure of FSWed joint of pure copper. It was observed that the pin with square profile had better recrystallized structure which ultimately results in better mechanical properties of copper welded joint in comparison with cylindrical with threaded pin. It is also reported that the ratio of swept to static volume plays major roles in deciding the plasticized flow of material associated with leading to trailing edge of the tool (Ref 19). The magnitude of plasticized material and its range decide the microstructure and hence the properties of the stirred zone (Ref 20). It has also been reported that profile of tool pin also affected the precipitation distribution in the welded zone. Elongated grains of the AA2024 after friction stir processing altered into fine-equiaxed grains, whereas micron- and tens of micron-sized precipitates observed in the as-received parent metal changed into 0.1-1micron-sized precipitates after friction stir processing/welding (FSP/W) (Ref 21). In experimental analysis, it was also analyzed that obtained grain refinement after FSP showed a detrimental effect on activation grain-boundary corrosion phenomenon as reported by Mehrian et al. (Ref 22). Satyanarayana and Kumar (Ref 23) investigated the effect of air, water and cryogenic cooling media on the grain refinement of FSWed AA2014 joints. It is observed from the

Bharat Singh, Kuldeep K. Saxena, and Piyush Singhal, Department of Mechanical Engineering, GLA University, Mathura, UP 281406, India; and **Tilak C. Joshi**, Advanced Construction Materials Division, CSIR-Advanced Materials and Processes Research Institute, Bhopal 462026, India. Contact e-mail: tilak@ampri.res.in.

EBSD analysis that underwater FSW showed fine grain structure and large fraction of high-angle grain boundaries (HAGB) in comparison with other media. Tamandon et al. (Ref 24) had examined the effect of conical, square and threaded tool pin profiles on the AA1100 alloys and found that the joint produced by threaded tool pin profile exhibits improved tensile strength and elongation. It was attributed that the uniform material flow in stirred zone by the threaded tool results in the improved tensile strength and ductility. Sabari et al. (Ref 25) studied the effect of pin profiles on FSWed joint of AA2519-T87 in underwater. Underwater FSWed joint made by taper with threaded pin profile exhibited better tensile properties with 76% joint efficiency (Ref 25). Enhancement in efficiency was attributed to uniform generation of heat during welding. Vijay and Murugan (Ref 26) had investigated the mechanical properties of metal matrix composite joined using friction stir welding. It was observed that the tensile strength of welded joint obtained using square pin was high in comparison with joints obtained by other tools. Alishavandi et al. (Ref 27) reported that cylindrical with threaded tool pin profile showed yielded tensile strength of AA1050 with 66% improvement, which was attributed to better severe plastic deformation and grain size reduction after FSP (Ref 27). Sharma et al. (Ref 28) have critically investigated the influence of FSW tool pin profile. Flat faces on lateral profile have more pulsating action which makes the ease in material flow and transport (Ref 28). Moreover, pulsating action results in grain size reduction and homogeneous redistribution, which leads to higher tensile strength and microhardness (Ref 7, 29).

Thus, a variety of pin profile tools are used to join the plates of different materials. But, very less or no work has been reported in the open literature to join the AA2024 material plates using different pin profile tools to know the best pin profile in order to provide better results. Therefore, in the present study, AA2024 plates are joined using different tool pin profiles to know the influence and best tool pin profiles on the joint in terms of mechanical properties and microstructural characterization.

2. Materials and Methods

The plate of AA2024 is procured from Bharat Aerospace Metals, Mumbai, Maharashtra, India. The plates are in the dimensions of 120 x 60 x 5 mm. The chemical composition of the as-received material AA2024 is given Table 1.

The mechanical properties of the as-received aluminum alloys AA2024 provided by Bharat Aerospace Metals, Mumbai, are as follows: density—2.78 g/cm³, young modulus—73GPa, UTS—462MPa, percentage elongation at break—18.5 and microhardness—132HV. The friction stir welding (FSW) is done of AA2024 plates in butt joint configuration using modified vertical milling machines setup.

A 3D model is shown in Fig. 1 to visualize the cross section of the various tool pin profiles along with their isometric views. The tool pin profiles are conical, pedal, cylindrical with thread, triangular, square and pentagonal in shape. The dynamic swept volume of all the pins is kept uniform. Moreover, other tool dimensions such as shoulder diameter, pin length and shoulder concavity are kept uniform in all the tool design. For the ease of understanding, each pin profile is designated with a unique code denoted as A, B, C, D, E and F simultaneously for conical, pedal, cylindrical with thread, triangular, square and pentagonal pin, respectively.

The friction stir welding of all samples using tool having different profiles is done considering the same welding input parameters. Joints are made by taking other input process parameters such as backing plate, plunge force, rotational speed, transverse speed and tilt angle uniform throughout the study, and they are given in Table 2.

The tools are fabricated from die steel AISI-H13. After machining of tools, heat treatment is done to increase and retain the hardness of the tool material. Therefore, all the machined tools from H13 die steel were heated slowly to austenitizing temperature, i.e., 1060 °C, as per the ASME standards (Ref 30) and soaked for half an hour at austenitizing temperature. Rapid oil marquenching is used to cool the tools. As a result, hardness of tools is found to be increased by 12 HRC. Before welding, faying surfaces of the samples are cleaned using acetone. The plate to be weld is firmly held together using a mechanically operated fixture to withstand the thrust and plunge force. Only defect-free welded samples are considered for further study. For mechanical testing and microstructural examination, welded joints are sectioned transversely (perpendicular to welding direction). Specimens for various testing, such as tensile, impact, microhardness and microstructure evaluation, are prepared as per the respective standard and extracted from the welded joint. A schematic diagram revealing the location and direction of specimen extraction from welded samples is shown in Fig. 2. ASTM E8 (2010) standard is followed for the tensile test specimen preparation. The tensile test samples are of 12.5 mm width with 60 mm gauge length cut transversely via wire cut EDM machine and tested on room temperature. To ensure the accuracy, five specimens were tested and three consistent results were taken for further analysis.

Microhardness testing on the prepared sample was conducted using the test load 0.2kg for 20 seconds. The five indentations were made around the joint at the mid-section of the plate thickness, and the best of three were taken for consideration. Impact strength of the prepared samples is measured using Charpy impact test. Test coupons are prepared as per American society for testing of materials standard ASTM E23.

For microstructural characterization, optical microscopy (OM), field-emission scanning electron microscope (FE-SEM), energy-dispersive spectroscopy (EDS) and electron backscatter diffraction (EBSD) measurements were used. Standard metallographic practice for sample preparation is

Table 1 Chemical composition of the as-received material AA2024 (wt.%)

Alloy	Cu	Fe	Si	Mn	Mg	Cr	Zn	Ti	Al
AA 2024	4.31–4.33	0.2	0.07	0.52	1.45–1.46	0.01	0.03	0.05	Balance

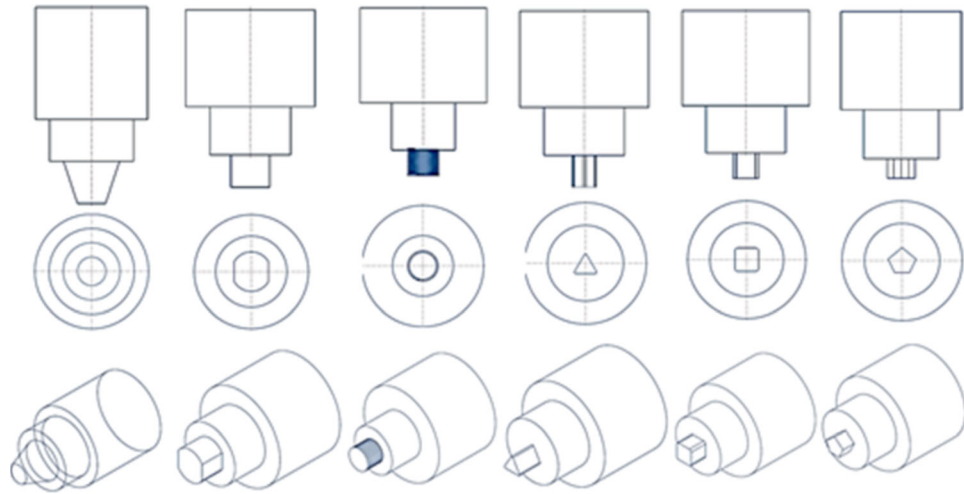


Fig. 1 A 3D model of various tool pin profiles showing the cross section and their isometric view, wherein A—conical pin, B—pedal pin, C—cylindrical with thread pin, D—triangular pin, E—square pin and F—pentagonal pin

Table 2 FSW input process parameters used for the joining

Parameters	Description	Unit
Tool material	Die steel (H13)	...
Shoulder concavity	2°	Degree
Shoulder diameter	24	mm
Tool pin length	4.2	mm
Backing plate material	Mild steel	...
Rotational speed	1025	rpm
Transverse speed	100	mm/min
Tilt angle	2°	Degree
Plunge force	3.5	kN

used. Etching of prepared and polished samples is done using Keller's reagents. Selected samples were used for FE-SEM, EDS and EBSD on the basis of optical images and mechanical properties. TSL OIM software is used to analyze the data obtained after the EBSD scan. For determining the various microstructural findings such as average grain size, grain boundaries distribution and angle of misorientation, at least 2000 grains were selected (Ref 31). The low-angle grain boundaries (LAGB) were identified with a misorientation angle between 5° and 15°, whereas misorientation angle > 15° was considered for high-angle grain boundaries.

3. Results and Discussion

Welded samples of AA2024 using different pin profiles tool are used for mechanical and microstructural characterization. The detail findings of mechanical properties and microstructural characterization are presented and discussed in the following section.

3.1 Influence of Pin Profile on Mechanical and Microstructural Properties

In FSW, tool pin profile directly affects material movement, heat generation and shearing action of plasticized materials during the process (Ref 7, 32). In the present study, different

tool pin profiles are used to understand the influence on mechanical properties and microstructural features. The detailed effects of pin design on the above-said properties are discussed in the following section.

3.1.1 Effect of Tool Pin Profile on Tensile Properties. After successful experiments, transverse tensile properties of samples are measured. Measured properties, which are UTS, joint efficiency and elongation (%), obtained through welding of samples using different tool pin profiles.

Figure 3 shows the true stress–true strain curves of tensile test of welded samples using different tool pin profiles. From Fig. 3, it is clear that the elongation and ultimate tensile strength (UTS) of as-received sample are highest among all tensile curves. The elongation and ultimate tensile strength (UTS) of as-received sample are 462 ± 5 MPa and 18.5%, respectively. All values of UTS and elongation are the average value of best three measurements. The UTS and elongation of all welded samples are found less compared to the as-received material, wherein least values of UTS and elongation are shown by samples welded using triangular pin, i.e., 285 MPa (UTS) and 7.9% (elongation) (see Fig. 3). Among all welded samples made by different tool pin profiles, joint made by square pin profile exhibits the higher UTS and percentage elongation values as shown in Fig. 4. Figure 4(a) shows the curve obtained through UTS values of samples welded using different tool pin profiles, whereas Fig. 4(b) reveals the elongation of all welded samples using varied tool pin profiles. The samples welded using square pin exhibited UTS as 362 MPa, and elongation is 15.1%. The UTS and elongation values of pedal pin-welded sample are more or less similar to square-pin-welded sample. The only difference is yield stress, which seems less as compared to square-pin-welded sample (see Fig. 3). The moderate values of UTS and elongations are represented by the samples welded using conical pin, pentagonal pin and cylindrical with thread pin. The UTS and elongation of conical-pin-welded sample are 324 MPa and 9.1%, respectively, whereas 304 MPa (UTS) and 11.29 (elongation) are observed from the welded sample using cylindrical with thread pin. Some considerable values of UTS and elongation are also exhibited by pentagonal-pin-welded sample, i.e., 334 MPa and 13.5%.

From Fig. 4, it is clear that the weld specimens showed low value of UTS and percentage elongation in comparison with as-

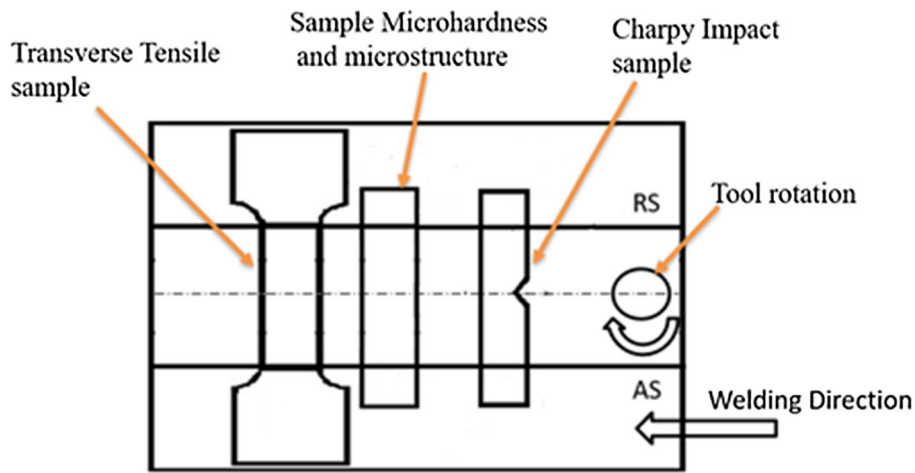


Fig. 2 Schematic diagram revealing the location and direction of specimen extraction from welded samples for mechanical and microstructural evaluation

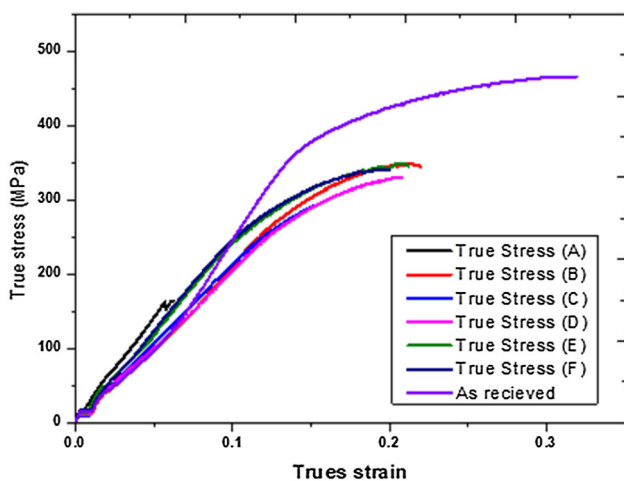


Fig. 3 True stress–strain curves obtained from tensile test of samples welded using different tool pin profiles

received material. It could be due to generation of heat and thus coarsening of precipitates (Al_2Cu) in developed HAZ region. Additionally, microstructure due to over-aging and localized deformation in the heat-affected zone reduced the tensile properties (transverse) of FSWed joints in terms of strength and ductility. In the case of FSWed joints, tensile fracture is exhibited on retreating side of the processing.

The fracture location is common in all welded samples regardless of tool pin profile. Most of the tensile samples fail by well-known shear mode, i.e., at 45° angle. The path of shear fracture was at 45° to axis of tensile load which corresponds to the lowest distribution of hardness profile (Ref 33). It could be attributed that the width of the soft zone of low value of hardness on advancing side (AS) is very low and the width of the low hardness value on retreating side (RS) is high. In general, it is also found that the failure occurs in a wide soft region (Ref 29).

The variation in the tensile results of different samples welded using different tool profiles could be due to a pulsating effect. A tool pin with flats exhibits significant material flow and pulsating action during FSW. Pulsating action of tools is accompanied by severe plastic deformation of material. It is

evident that in FSW process, the generation of heat is result of severe and rapid plastic deformation and frictional heating (Ref 7). In order to attain the desired peak temperature, sufficient heat generation at the interfaces is needed. It is attributed that welding with tool triangular pin takes longer time to achieve the peak temperature. Thus, more heat is conducted through plate and widens the region of TMAZ and HAZ (Ref 29). Therefore, the loss of heat in the stirred zone results in insufficient dynamic recrystallization and hence joint formed showed lower strength and poor joint efficiency. In particular, in square pin profile, higher-temperature and plasticized material is obtained by pulsating action of sharp flats and associated frictional heating. As a result, uniform microstructure across the welded region is revealed, which is due to thoroughly worked region. Among all six samples, samples welded using square pin showed superior tensile properties (Fig. 4) with 78% joints efficiency (see Fig. 5a). Though the UTS results are showing lower values than those of the as-received material, the joint performance is much higher than that obtained by other traditional processes of fusion welding (Ref 12, 34).

The other traditional processes of fusion welding are arc welding processes (TIG) associated with high heat input. The heat input associated with fusion welding process leads to high softening of aluminum with high residual stresses, resulting in distortion of the part (Ref 4, 5). High thermal conductivity, coefficient of thermal expansion and reactivity make aluminum alloys difficult to weld aluminum alloys using traditional welding process, and it show poor strength in comparison with FSW process.

3.1.2 Microhardness Variation with Tool Pin Profiles. The other mechanical property, which is greatly affected by welding of two parts, is hardness. Therefore, the influence of different tool pin profiles on welded material's microhardness is recorded by Vickers microhardness tester. The microhardness values of welded samples are shown in Fig. 5(b). The symbolic representation of the indentation during hardness measurement is given in the inset of Fig. 5(b). Figure 5(b) clearly reveals that the microhardness results are greatly influenced by the design and geometry of the FSW tool pin profile. The microhardness patterns across weld region can be attributed with heat distribution trends. Result of microhardness can be interpreted that a softened region shows low-hardness distribution region

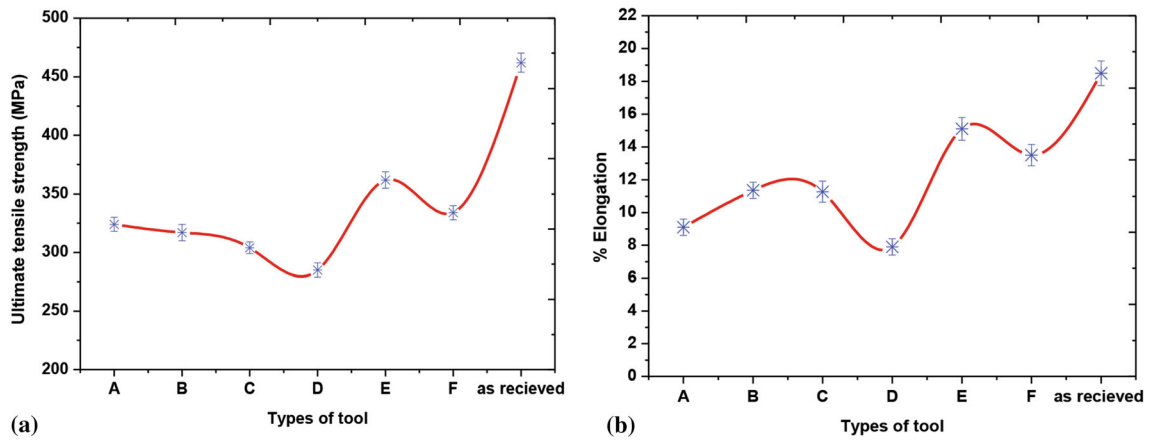


Fig. 4 Results of tensile test of samples welded using different pin profiles: (a) (UTS) and (b) elongation (%)

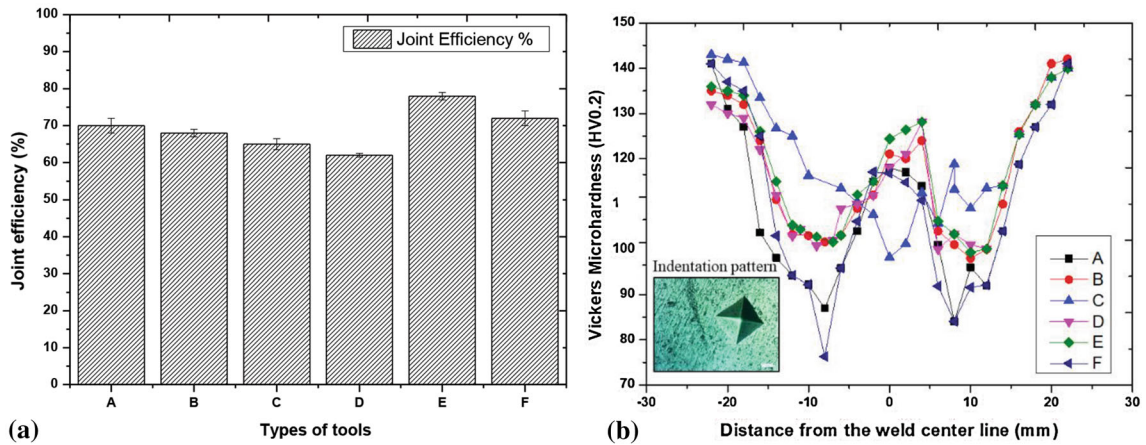


Fig. 5 Variation of obtained properties of welded samples by different tool pin profiles: (a) joint efficiency; (b) micro-Vickers hardness

(LHDR) found across the weld. Observed softened region of weld zone occurs due to dynamic recrystallization which diminishes the effect of strain hardening. In general, all welded samples for microhardness using different pin profile showing W shaped hardness graphs across the welds. Among the different regions, thermo-mechanically affected zone (TMAZ) reported lower hardness on both the advancing and retreating side of the joints. From Fig. 5(b), it is clear that the microhardness of the as-received material is measured as 132 ± 5 HV0.2. It is observed from measured values of microhardness that stir zone shows higher value of microhardness among the all regions of welded joint except the as-received material. Among all tool samples, there is significant loss in the hardness of welded region using C tool pin profile (triangular pin) in comparison with as-received material.

The best hardness characteristics among all samples are shown by sample welded using tool pin E (square pin profile). Stir zone (SZ) using tool pin E possesses 113 HV0.2 microhardness, which is 14% lower than the parent metal. It is also examined that among the different regions, TMAZ reported lower hardness on the advancing and retreating side of the joints. The HAZ showed low values of hardness in comparison with as-received material, but it is higher than the TMAZ. Low-hardness regions are the consequences of dissolution of the Al_2Cu precipitates during friction stir welding (Ref 35). The impact of grain size is also evident in the SZ, provided the various hardening mechanisms can work on such

kind of alloy. In the contact zone of the tool, high values of peak temperature in the SZ result in heterogeneous distribution of grain size. It can be attributed that the grain size decreases from top to bottom of the welded joint. Similar observations are found by Dixit et al. (Ref 2). In the same context, the distribution of precipitates is different in the various regions of welding such as HAZ, TMAZ and SZ. The distribution of precipitates can be attributed as the dissolution of the precipitates depends upon the peak temperature reached and extent of deformation in the zone. Therefore, the coalesce of the precipitates results in coarsening of precipitates which reduced hardness and strength of the welded region. Thus, the lower hardness and strength findings are result of the dissolution and re-dispersion of the precipitates, wherein the growth of the precipitates is responsible for bond strength relative to those of the as-received material.

3.1.3 Impact Strength of FSWed Joint Developed by Various Tool Pin Profiles. Impact strength of a material shows its toughness or resistance offered by material till its failure. The impact strength is greatly influenced by welding of the two components using different input process parameters. Furthermore, the influences of different tool pin profiles on impact energy of welded joints are investigated. In the present work, the impact strength of samples welded using different tool pin profiles are obtained using Charpy impact test. The Charpy impact test results in terms of impact strength are shown in

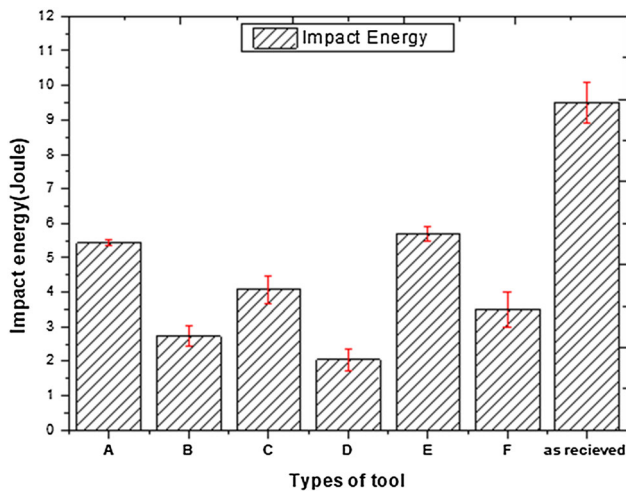


Fig. 6 Impact energy variation with different tool pin profiles

Fig. 6. It is clear from Fig. 6 that the trends of the impact energy results are more or less similar to tensile properties results of the studied material. It can be seen from the results that all welded samples exhibit as usual lower impact energy in comparison with the as-received material. The impact energy of the as-received material is measured as 9.5 joule. Among all pin profiles, the lowest impact energy is found of joint with tool D (triangular pin), i.e., 2.72 joule which is 70% lower than the parent metal as shown in Fig. 6, whereas the impact energy of sample welded with tool E is measured to be 5.7 joule. The impact energy values obtained of joint using square pin profile are higher than the impact energy recorded of all welded samples using different tools, i.e., A, B, C, D and F. The change in impact strength could be due to maximum dynamic recrystallization, and dispersion of precipitates of joint made by square pin results in higher toughness or impact energy.

Based on the tensile properties, microhardness and impact energy results, it can be concluded that the tool having square pin profile provides and contributes to better material flow during the FSW process. Additionally, joint made by square pin profile showed higher mechanical properties in comparison with other tool pin profile joints. It is also observed that defect-free joint is obtained with higher joint efficiency using square pin profile. To know the more significant contribution of square pin profile, in-depth microstructural analysis of samples welded using square pin profile is required. The in-depth microstructural analysis of samples welded using square pin profile is shown and discussed in the following section.

3.2 Microstructural Analysis

In any processing, the end microstructure plays a significant role in various properties such as mechanical properties etc. In the similar context, microstructure of material welded through FSW technique also has an influence of various processing parameters. The effect of selected parameters on microstructure of FSWed samples is discussed in the following section. Figure 7 shows the cross-sectional plane of welded joint showing various regions observed after FSW. It can be observed that the joints are free from any discontinuities and show adequate plasticized material flow. The processed region using FSW is further divided as stir zone or nugget zone, TMAZ, HAZ and unaffected parent metal. Usually, it is found that the microstruc-



Fig. 7 Cross-sectional plane of welded joint showing various zones of square pin friction stir-welded AA2024

ture of thermo-mechanically affected zone (TMAZ) exhibits twisted and elongated grains, just after the nugget zone where no shearing of material occurred. It is found that the grains are stretched upward in TMAZ which is parallel to the direction of material flow. In TMAZ, recrystallization process is not significantly affected to achieve the plastic deformation (Ref 36). Depending on the geometry of the tool and the welding conditions, various zones of the friction stir weld are subject to different thermal loadings. Compared to HAZ and TMAZ, smaller, nearly equiaxed grains were observed in the weld stirred zone (Ref 37).

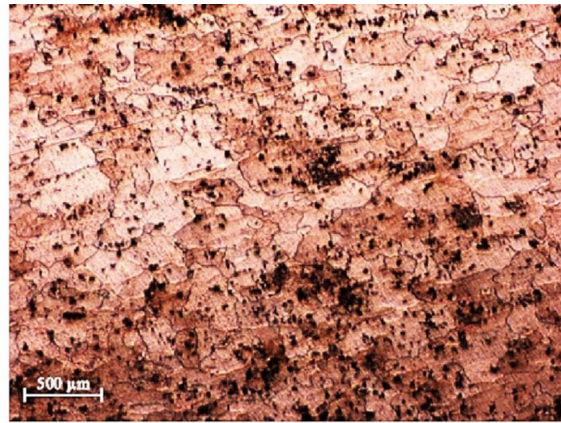
The micrograph of processes and the as-received material is shown in Fig. 8, wherein Fig. 8(a) shows the microstructure of the as-received base metal, whereas Fig. 8(b) shows the microstructure of stirred zone of FSWed sample and intermetallic compound in the stirred zone is shown in Fig. 8(c). From Fig. 8(b), onion rings (i.e., a kind of layered structure) are formed at the bottom of the weld during the FSW process. The formation of onion rings is due to the rotation of the tool. Such features of onion rings are formed by the shearing of thin layer during the FSW. Another supporting reason for the onion rings development is heat generation in the welded region due to rotation of tool and its forward movement with the extruded material around FSW tool.

Similar onion rings formation is also reported by other study during the FSW process (Ref 38). Figure 8(c) shows the microstructure of welded region specially nugget zone or stir zone. In Fig. 8(c), some appearance of precipitates formation is shown. Precipitation and their uniform distribution play a key role in deciding the mechanical properties (Ref 39). The formed precipitate could be of Al_2Cu , wherein the distribution of such precipitates is less uniform in some locations (see Fig. 8c).

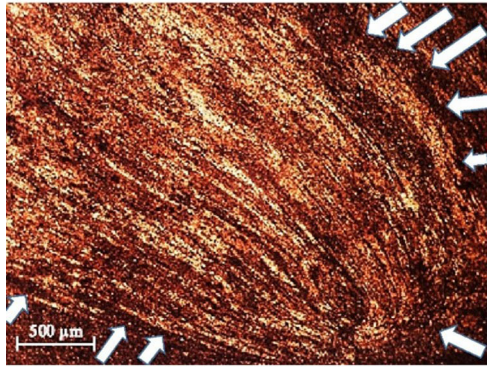
But, it is difficult to identify the precipitates through optical micrograph for the studied alloy; therefore, FESEM image has been shown to reveal the precipitation in the stir zone. Figure 9(a) shows the FESEM image of stir zone, wherein bright patches seem to be precipitates. In order to confirm that the bright patches are the precipitates, EDS analysis is carried out. EDS analysis image (Fig. 9b) reveals that the bright patches are precipitates having elemental composition of approximately Al—90.13%, Cu—8.3%, and very less amount of Mg—0.93%.

3.3 EBSD Analysis of the Joint Developed by Square Pin Profile Tool

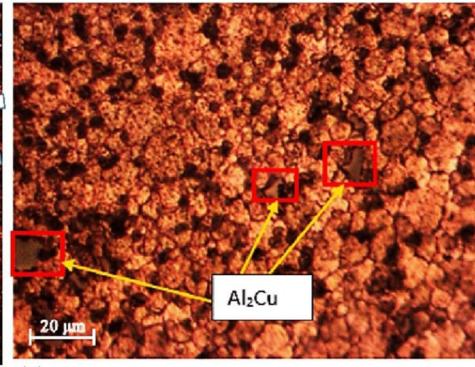
To know the in-depth information from the microstructure such as grain size and low/high angle grain boundaries, EBSD measurement was taken for the selected weld joint. The selected weld joint is the weld joint welded using square pin profile. Various pieces of information such as grain size, misorientation angle and high/low angle grain boundaries are obtained from EBSD measurements. Figure 10 shows the inverse pole figure (IPF) map of different locations for weld



(a)

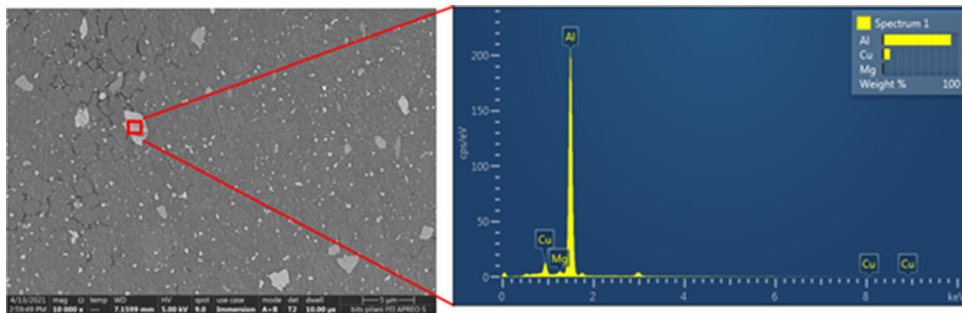


(b)



(c)

Fig. 8 Optical micrograph of FSWed joint using square tool pin profile showing (a) base metal, (b) stirred zone and (c) intermetallic compound in the stirred zone



(a)

(b)

Fig. 9 SEM image of stir zone with EDS elemental distribution analysis: (a) FESEM image showing the distribution of precipitates in SZ and (b) EDS elemental analysis

joint done using the square pin profile. The different zones of weld joints such as stir zone or nugget zone, TMAZ, HAZ and unaffected parent metal are shown in Fig. 10(a). The IPF map of nugget zone is shown in Fig. 10(c), wherein recrystallization of new grains is clearly visible after the process. Additionally, significant volume of equiaxed grains is also evident in the IPF map of nugget zone. Very less percentage of deformed grains are observed in nugget zone (Fig. 10c). The orientation of recrystallized grain and deformed grains is totally different with each other. The IPF map of HAZ region of retreating and advancing side is shown in Fig. 10(b) and (d), respectively. From both the figures (i.e., Fig. 10b and d), it is clear that the grains are more elongated in the HAZ region of retreating side

(Fig. 10b), whereas in advancing side HAZ region elongation is not observed in the grain of IPF map (Fig. 10d). Additionally, some small equiaxed grains are also visible at the junction of deformed grains specially in advancing side HAZ region, whereas no such grains are visible in retreating side. It is observed that stirred zone microstructure mainly exhibits high-angle grain boundaries with very less sub grains. Local variation of the grain size appears in the considerably in the structure as shown in Fig. 10. Obtained microstructure of the stirred zone is dynamically recrystallized. Similar trends of grain size reduction are also reported in stirring zone (40, 41).

To understand the influence of square pin profile tool on weld joint, especially the material flow, grain boundary analysis

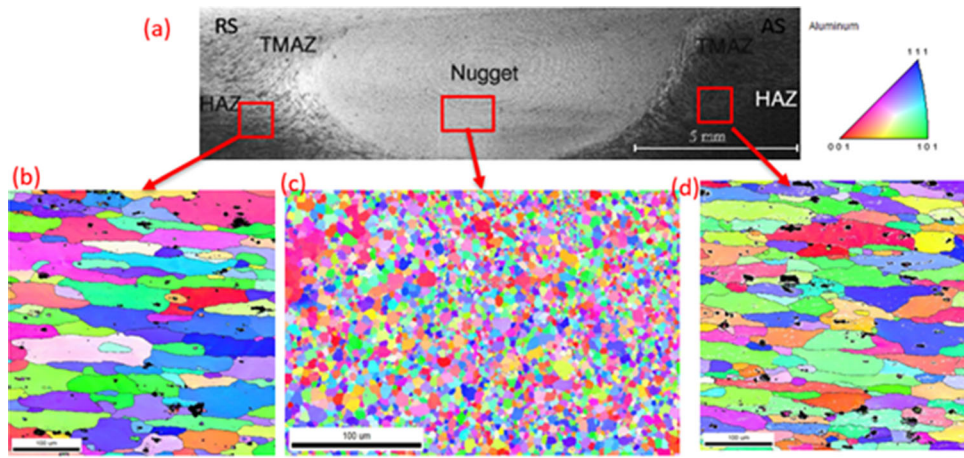


Fig. 10 EBSD micrograph of FSWed joint showing different zones: (a) macrostructure of the joint, (b) RS-HAZ, (c) SZ and (d) AS-HA

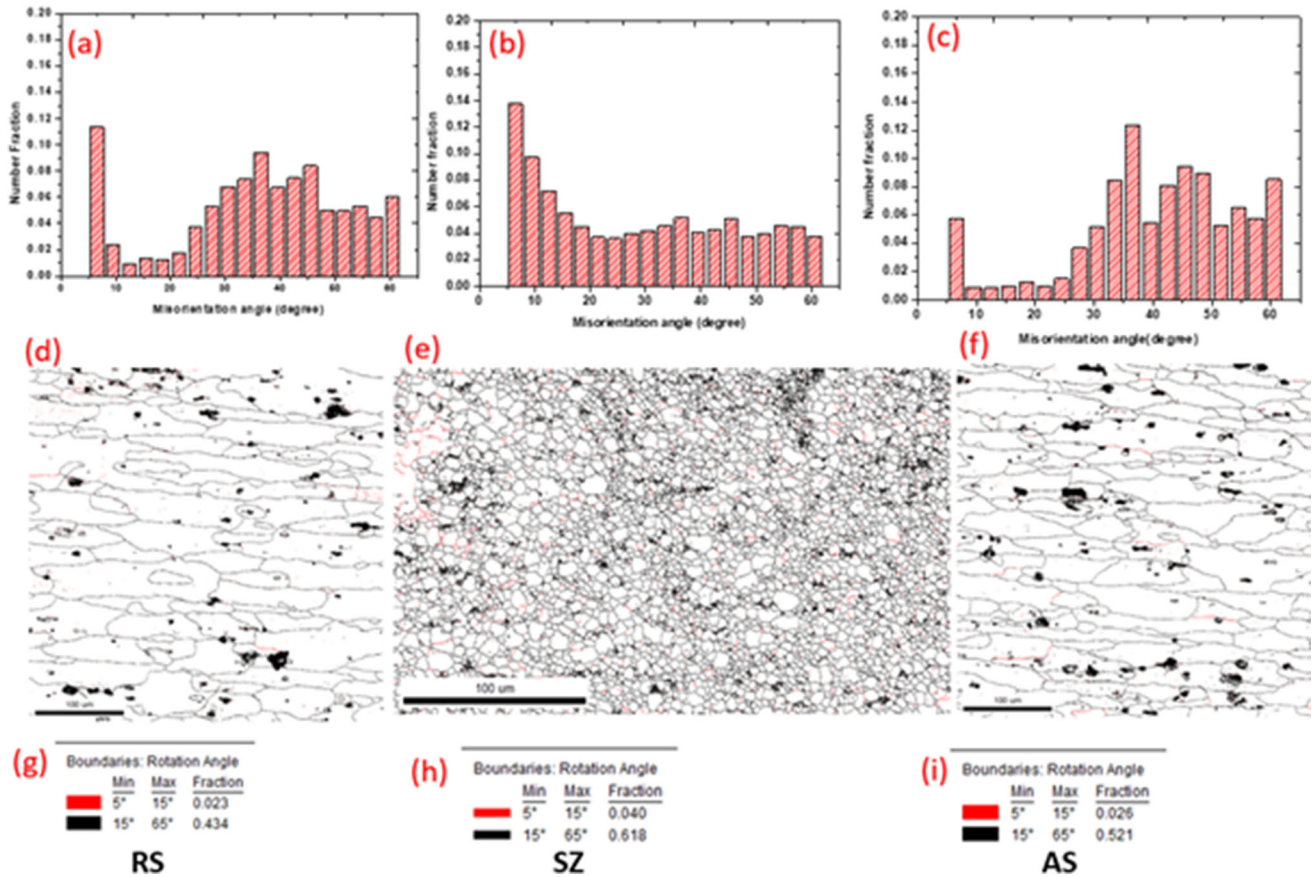


Fig. 11 EBSD measurements data of sample welded using square tool pin profile; (a) misorientation angle in RS region, (b) misorientation angle in SZ region, (c) misorientation angle in AS region, (d) grain boundary map of RS region with high- and low-angle boundaries (LAGBs/HAGBs) (key and fraction is shown in Fig. (g)), (e) grain boundary map of SZ region with high- and low-angle boundaries (key and fraction is shown in Fig. (h)) and (f) grain boundary map of AS region with high- and low-angle boundaries (key is shown in Fig. i).

is done on all three domains such as stir region and HAZ of AS and RS. The grain boundary maps are shown in Fig. 10. In grain boundaries maps, low-angle grain boundaries (LAGB) and high-angle grain boundaries (HAGB) are shown by red and black lines, respectively.

In the present study, grains are defined as the small entity exhibiting a misorientation 5° or more with its neighbor entity. Based on the above-mentioned criteria, the distribution of

misorientation angles between the grain boundaries were identified and calculated. The misorientation angle of grain boundaries between 5° and 15° is termed as low-angle grain boundaries (LAGB), whereas grain boundaries with misorientation angle greater than 15° are considered as high-angle grain boundaries (Ref 42). However, random distribution of sub-grains can be seen in the microstructure, which can be specified with angle less than the 5° . In grain boundary map (Fig. 11e), large fraction of

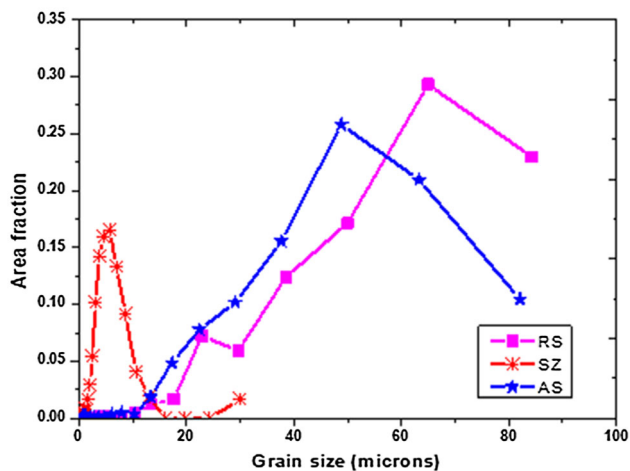


Fig. 12 Grain size–area fraction graph of FSWed joint in different weld zones as RS-HAZ, AS-HAZ and SZ

high-angle grain boundaries in stir zone is observed. From Fig. 11(h), it is clear that the fraction of HAGB is 61% in the stir zone, which is a significant indication of new recrystallized and refined grains. The refinement of grain size can also be observed from Fig. 11(e). The number fraction of misorientation angle corresponding region, i.e., stirring zone is shown in Fig. 11(b). From Fig. 11(b), it can be attributed that whatever appearance of grains in stirring region is a kind of recrystallized grains, whereas Fig. 11(a) and (b) represents the number fractions of misorientation angle of RS and AS regions, respectively. From Fig. 11(a) and (g), it is clear that the fraction of recrystallized grain in RS region is very nominal and mostly deformed grains could be there. The indication of deformed grains from Fig. 11(a) and (g) is quite confirmed with the grain boundary map shown in Fig. 11(d). Figure 11(d) clearly reveals the elongated grains in RS region. Such elongated grain could be attributed due to the generation of less heat during the process. Similar kinds of features are also obtained in AS side as shown in Fig. 11(c), (f) and (i) for fraction of misorientation angle, grain boundary map and fraction of high- and low-angle grain boundaries. Additionally, it is clear from Fig. 12 that the HAGB fraction is more in HAZ-AS in comparison with RS. Figure 12 shows the area fraction of grain size of sample joined using square pin profile. It is clear from the figure that stir zone (SZ) possesses major area fraction of grain size between 3.5 μm and 8.5 μm . The average grain size in the stirred zone was observed as 5.1 μm . The grain size obtained in SZ is smaller than the average grains size of AS-HAZ and RS-HAZ. Smaller grain size in the structure could be attributed to have better strength of the material as per the well-known Hall–Petch equation (Ref 43, 44).

It is found that continuous dynamic recrystallization (CDRX) majorly occurs in high stacking fault energy materials and encourage the formation of new grains the progressive increase in low angle boundary misorientations (Ref 45). Continuous increase in misorientation angle results in formation of HAGB in the structure. Improved strain hardening is observed in structure with high fraction of HAGB. It is well examined that the HAGBs block and hinder the movement of dislocations significantly. Thus, capacity of strain hardening increased which results in improved strength and ductility of the joint (Ref 46). The grain size obtained from microstructural analysis also validates the Hall–Petch equation with dislocation

density. The relation of grain size with Hall–Petch equation is the quite visible in mechanical properties. The Hall–Petch equation plays vital role in deciding the strength and hardness of the joint (Ref 47). Even, fine structure of the FSWed joint exhibits less strength in comparison with parent metal. It is because of the dislocation density phenomenon, which is more dominant in determining the strength of materials. Due to stirring action and dynamic recrystallization, dislocation density significantly decreased in the structure which results in loss of strength.

4. Conclusions

The present work compiles the influence of different pin profile on the weld characteristics of AA2024 in terms of microstructural change and their effect on mechanical properties. The best tool pin profile was obtained from the mechanical properties of joints, welded using different pin profile. Conclusions drawn from the above study are as follows:

1. The square tool pin profile provides better mechanical properties of the FSWed joint in comparison with other tool pin profiles such as conical, pedal, cylindrical with thread, triangular and pentagonal tool.
2. The joint made by tool with square pin profile exhibited 78% joint efficiency. The UTS, percentage elongation and impact energy are obtained as 362 MPa, 15% and 5.7 Joule, respectively.
3. The pulsating action due to flat faces of the square tool provides better material flow and high heat generation and thus the development of more recrystallized microstructure, which improves the overall properties of the welded joint.
4. The grain size obtained in SZ is smaller than the average grains size of AS-HAZ and RS-HAZ.
5. Electron backscattering diffraction (EBSD) analysis also revealed that the stirred zone (SZ) exhibits the recrystallized fine-equiaxed grains, which is a result of dynamic recrystallization.

References

1. I.G. Crouch, Body Armour—New Materials, New Systems, *Def. Technol.*, 2019, **15**(3), p 241–253
2. V. Dixit, R.S. Mishra, R.J. Lederich and R. Talwar, Influence of Process Parameters on Microstructural Evolution and Mechanical Properties in Friction Stirred Al-2024 (T3) Alloy, *Sci. Technol. Weld. Join.*, 2009, **14**(4), p 346–355
3. B. Singh, P. Singhal and K.K. Saxena, Effect of Transverse Speed on Mechanical and Microstructural Properties of Friction Stir Welded Aluminium AA2024-T351, *Adv. Mater. Process. Technol.*, 2020, **6**, p 519
4. B. Singh, P. Singhal, K.K. Saxena, R.K. Saxena, Influences of Latent Heat on Temperature Field, Weld Bead Dimensions and Melting Efficiency During Welding Simulation, *Met. Mater. Int.*, 2020
5. W.-C. Dong, D.-B. Gao and S.-P. Lu, Numerical Investigation on Residual Stresses of the Safe-End/Nozzle Dissimilar Metal Welded Joint In CAP1400 Nuclear Power Plants, *Acta Metallurgica Sinica (English Letters)*, 2019, **32**(5), p 618–628

6. W. M. Thomas, E. D. Nicholas, J. C. Needham, M. G. Murch, P. Temple-Smith, C. J. Dawes, Friction Stir Butt Welding, *GB Patent No. 9125978.8.*, (1991)
7. K. Elangovan, V. Balasubramanian and M. Valliappan, Effect of Tool Pin Profile and Tool Rotational Speed on Mechanical Properties of Friction Stir Welded AA6061 Aluminium Alloy, *Mater. Manuf. Process.*, 2008, **23**(3), p 251–260
8. A. Goyal and R.K. Garg, Effect of Tool Rotational and Transverse Speed on Mechanical Properties of Friction Stir Welded AA5086-H32 Aluminium Alloy, *Int. J. Microstruct. Mater. Prop.*, 2017, **12**(1–2), p 79–93
9. S. Kumar, U. Acharya, D. Sethi, T. Medhi, B.S. Roy and S.C. Saha, Effect of Traverse Speed on Microstructure and Mechanical Properties of Friction-Stir-Welded Third-Generation Al-Li Alloy, *J. Braz. Soc. Mech. Sci. Eng.*, 2020, **42**(8), p 423
10. Y. Sarikavak, An Advanced Modelling to Improve the Prediction of Thermal Distribution in Friction Stir Welding (FSW) for Difficult to Weld Materials, *J. Braz. Soc. Mech. Sci. Eng.*, 2020, **43**(1), p 4
11. S. Emamian, M. Awang, F. Yusof, P. Hussain, B. Meyghani and A. Zafar, The Effect of Pin Profiles and Process Parameters on Temperature and Tensile Strength in Friction Stir Welding of AL6061 Alloy, *The Advances in Joining Technology*. M. Awang Ed., Springer, Singapore, 2019, p 15–37
12. G. Çam and G. İpekoğlu, Recent Developments in Joining of Aluminum Alloys, *Int. J. Adv. Manuf. Technol.*, 2017, **91**, p 1851–1866
13. X. Li, X. Wang, Z. Liang and D. Wang, Influence of FSW Repairing Process on the Microstructures and Mechanical Properties of Friction Stir-Welded 6082Al Alloy, *J. Mater. Eng. Perform.*, 2019, **28**(9), p 5299–5306
14. R.S. Mishra and Z.Y. Ma, Friction Stir Welding and Processing, *Mater. Sci. Eng. R. Rep.*, 2005, **50**(1), p 1–78
15. G. Cantin, S. David, W. Thomas, E. Lara-Curzio and S. Babu, Friction Skew-Stir Welding of Lap Joints in 5083-0 Aluminium, *Sci. Technol. Weld. Join.*, 2005, **10**, p 268–280
16. R. Rai, A. De, H.K.D.H. Bhadeshia and T. DebRoy, Review: Friction Stir Welding Tools, *Sci. Technol. Weld. Join.*, 2011, **16**(4), p 325–342
17. Z. Dong, K. Yang, R. Ren, G. Wang, L. Wang and Z. Lv, Friction Stir Lap Welding 0.8-mm-thick 2024 Aluminum Alloy with the Assistance of Stationary Shoulder, *J. Mater. Eng. Perform.*, 2019, **28**(11), p 6704–6713
18. H. Khodaverdizadeh, A. Heidarzadeh and T. Saeid, Effect of Tool Pin Profile on Microstructure and Mechanical Properties of Friction Stir Welded Pure Copper Joints, *Mater. Des.*, 2013, **45**, p 265–270
19. V.P. Singh, S.K. Patel, A. Ranjan and B. Kuriachen, Recent Research Progress in Solid State Friction-Stir Welding of Aluminium-Magnesium Alloys: A Critical Review, *J. Market. Res.*, 2020, **9**(3), p 6217–6256
20. G. Ghangas and S. Singhal, Effect of Tool Pin Profile and Dimensions on Mechanical Properties and Microstructure of Friction Stir Welded Armor Alloy, *Mater. Res. Express*, 2018, **5**(6), p 066555
21. M. Regev and S. Spigarelli, Microstructure, Thermal Stability During Creep and Fractography Study of Friction-Stir-Processed AA2024-T3 Aluminum Alloy, *J. Mater. Eng. Perform.*, 2020, **29**(8), p 4872–4878
22. S.S.M. Mehrian, M. Rahsepar, F. Khodabakhshi and A.P. Gerlich, Effects of Friction Stir Processing on the Microstructure, Mechanical and Corrosion Behaviors of an Aluminum-Magnesium Alloy, *Surf. Coat. Technol.*, 2021, **405**, p 126647
23. M. Satyanarayana and A. Kumar, Influence of Cooling Media in Achieving Grain Refinement of AA2014 Alloy Using Friction Stir Processing, *Proc. Inst. Mech. Eng. C J. Mech. Eng. Sci.*, 2020, **234**(22), p 4520–4534
24. A. Tamadon, A. Baghestani and M.E. Bajgholi, Influence of WC-based Pin Tool Profile on Microstructure and Mechanical Properties of AA1100 FSW Welds, *Technologies*, 2020, **8**(2), p 34
25. S.S. Sabari, S. Malarvizhi and V. Balasubramanian, The Effect of Pin Profiles on the Microstructure and Mechanical Properties of Underwater Friction Stir Welded AA2519-T87 Aluminium Alloy, *Int. J. Mech. Mater. Eng.*, 2016, **11**(1), p 5
26. V. Santhiyagu and N. Murugan, Influence of Tool Pin Profile on the Metallurgical and Mechanical Properties of Friction Stir Welded Al–10 wt.% TiB₂ Metal Matrix Composite, *Mater. Des.*, 2010, **31**, p 3585–3589
27. M. Alishavandi, M. Ebadi, A.H. Kokabi, Optimization of Parameters for the Friction Stir Processing and Welding of AA1050 Aluminum Alloy, 2021
28. N. Sharma, A.N. Siddiquee, Z.A. Khan and M.T. Mohammed, Material Stirring During FSW of Al-Cu: Effect of Pin Profile, *Mater. Manuf. Process.*, 2018, **33**(7), p 786–794
29. K. Ramanjaneyulu, G. Madhusudhan Reddy, A. Venugopal Rao and R. Markandeya, Structure-Property Correlation of AA2014 Friction Stir Welds: Role of Tool Pin Profile, *J. Mater. Eng. Perform.*, 2013, **22**(8), p 2224–2240
30. ASM International, *ASM Handbook—Heat Treating* **4**, 1991
31. K.A. Babu, S. Mandal, A. Kumar, C.N. Athreya, B. de Boer and V.S. Sarma, Characterization of Hot Deformation Behavior of Alloy 617 Through Kinetic Analysis, Dynamic Material Modeling and Microstructural Studies, *Mater. Sci. Eng. A*, 2016, **664**, p 177–187
32. A.N. Chaudhari, K. Dixit, G.S. Bhatia, B. Singh, P. Singhal and K.K. Saxena, Welding Behaviour of Duplex Stainless Steel AISI 2205: A Review, *Mater. Today Proc.*, 2019, **18**, p 2731–2737
33. S.R. Ren, Z.Y. Ma and L.Q. Chen, Effect of Welding Parameters on Tensile Properties and Fracture Behavior of Friction Stir Welded Al-Mg-Si Alloy, *Scripta Mater.*, 2007, **56**(1), p 69–72
34. K. Vasu, H. Chelladurai, A. Ramaswamy, S. Malarvizhi and V. Balasubramanian, Effect of Fusion Welding Processes on Tensile Properties of Armor Grade, High Thickness, Non-Heat Treatable Aluminium Alloy Joints, *Def. Technol.*, 2019, **15**(3), p 353–362
35. Y.S. Sato, H. Kokawa, M. Enomoto and S. Jogan, Microstructural Evolution of 6063 Aluminum During Friction-Stir Welding, *Metall. Mater. Trans. A.*, 1999, **30**(9), p 2429–2437
36. J. John, S.P. Shanmuganatan, M.B. Kiran, V.S. Senthil Kumar and R. Krishnamurthy, Investigation of Friction Stir Processing Effect on AA 2014-T6, *Mater. Manuf. Process.*, 2019, **34**(2), p 159–176
37. D.K. Yaduwanshi, S. Bag and S. Pal, On the Effect of Tool Offset in Hybrid-FSW of Copper-Aluminium Alloy, *Mater. Manuf. Process.*, 2018, **33**(3), p 277–287
38. I. Radisavljevic, A. Zivkovic, N. Radovic and V. Grabulov, Influence of FSW Parameters on Formation Quality and Mechanical Properties of Al 2024-T351 Butt Welded Joints, *Trans. Nonferrous Met. Soc. China*, 2013, **23**(12), p 3525–3539
39. J.H. Kim, F. Barlat, C. Kim and K. Chung, Thermo-Mechanical and Microstructural Modeling of Friction Stir Welding of 6111-T4 Aluminum Alloys, *Met. Mater. Int.*, 2009, **15**(1), p 125
40. Y. Li, D. Sun and W. Gong, Effect of Tool Rotational Speed on the Microstructure and Mechanical Properties of Bobbin Tool Friction Stir Welded 6082–T6 Aluminum Alloy, *Metals*, 2019, **9**, p 894
41. G. Ugrasen, G. Bharath, G.K. Kumar, R. Sagar, P.R. Shivu and R. Keshavamurthy, Optimization of Process Parameters for Al6061-Al7075 Alloys in Friction Stir Welding Using Taguchi's Technique, *Mater. Today Proc.*, 2018, **5**(1 Part 3), p 3027–3035
42. A. Malakar, K.S. Suresh, V. Pancholi, H.-G. Brokmeier and N. Schell, Texture Transition in Friction Stir Processed Al Powder Compact, *Mater. Charact.*, 2020, **167**, p 110525
43. Z.C. Cordero, B.E. Knight and C.A. Schuh, Six Decades of the Hall–Petch Effect—A Survey of Grain-Size Strengthening Studies on Pure Metals, *Int. Mater. Rev.*, 2016, **61**(8), p 495–512
44. W. Woo, L. Balogh, T. Ungár, H. Choo and Z. Feng, Grain Structure and Dislocation Density Measurements in a Friction-Stir Welded Aluminum Alloy Using x-ray Peak Profile Analysis, *Mater. Sci. Eng. A*, 2008, **498**, p 308–313
45. S. Gourdet and F. Montheillet, A Model of Continuous Dynamic Recrystallization, *Acta Mater.*, 2003, **51**, p 2685–2699
46. Y.H. Zhao, Y. Zhu and E. Lavernia, Preparation of Nanostructured Materials Having Improved Ductility, *Adv. Eng. Mater.*, 2010, **12**, p 769–788
47. S.N. Naik and S.M. Walley, The Hall–Petch and Inverse Hall–Petch Relations and the Hardness of Nanocrystalline Metals, *J. Mater. Sci.*, 2020, **55**(7), p 2661–2681

Publisher's Note Springer Nature remains neutral with regard to jurisdictional claims in published maps and institutional affiliations.